



ELSEVIER

Available online at www.sciencedirect.com

SCIENCE @ DIRECT®

Nuclear Instruments and Methods in Physics Research A 545 (2005) 643–657

NUCLEAR
INSTRUMENTS
& METHODS
IN PHYSICS
RESEARCH
Section A

www.elsevier.com/locate/nima

A large area muon tracking detector for ultra-high energy cosmic ray astrophysics—the GRAPES-3 experiment

Y. Hayashi^a, Y. Aikawa^a, N.V. Gopalakrishnan^b, S.K. Gupta^{b,*}, N. Ikeda^a, N. Ito^a, A. Jain^b, A.V. John^b, S. Karthikeyan^b, S. Kawakami^a, H. Kojima^c, T. Matsuyama^a, D.K. Mohanty^b, P.K. Mohanty^b, S.D. Morris^b, T. Nonaka^a, A. Oshima^a, B.S. Rao^b, K.C. Ravindran^b, M. Sasano^a, K. Sivaprasad^b, B.V. Sreekantan^b, H. Tanaka^a, S.C. Tonwar^b, K. Viswanathan^b, T. Yoshikoshi^a

^aGraduate School of Science, Osaka City University, Osaka 558-8585, Japan

^bTata Institute of Fundamental Research, Mumbai 400 005, India

^cNagoya Women's University, Nagoya 467-8610, Japan

Received 1 November 2004; received in revised form 26 January 2005; accepted 9 February 2005

Available online 15 April 2005

(The GRAPES-3 Collaboration)

Abstract

Certain aspects of ultra-high energy (UHE) cosmic ray astrophysics require correlated studies on the electron and muon components of air showers, namely, the search for cosmic ray sources through γ -ray astronomy and studies on the variation of the nuclear composition of primary cosmic rays with energy. While studies on the electron component provide basic information about the arrival direction and energy, it is the muon component that plays a crucial role in distinguishing primary γ -rays from charged cosmic ray particles and in determining the composition.

A large area (560 m²), tracking muon detector of the GRAPES-3 experiment, operating at Ooty in southern India, has been designed for detailed studies on both of these aspects of UHE cosmic ray astrophysics. We present here the details of the muon detector, associated electronics and the data acquisition system. A brief discussion of the potential of the muon detector is presented through simulation studies.

© 2005 Elsevier B.V. All rights reserved.

PACS: 98.70.Sa; 96.40.Pq; 96.40.De; 98.70.Rz; 95.55.Vj; 13.85.Tp

Keywords: Cosmic rays; Extensive air showers; Composition; Energy spectra and interactions; Gamma-ray sources; Cosmic ray detectors; Cosmic ray interactions

*Corresponding author. Tel.: +91 22 2280 4545; fax: +91 22 2280 4610.

E-mail address: gupta@grapes.tifr.res.in (S.K. Gupta).

1. Introduction

Cosmic rays span an enormous range of energy from $\sim 10^8$ eV to beyond 10^{20} eV with an energy spectrum that is essentially a continuous power law. The high interest in cosmic ray astrophysics [1] continues to be driven by the fact that it is almost impossible to understand all the available information on high energy cosmic rays through known acceleration processes and nature of astrophysical sources. Owing to the deflection of charged cosmic rays by the randomly oriented interstellar magnetic fields, the cosmic ray flux incident on the Earth is highly isotropic and loses all the information about the sources and their directions. Acceleration [2,3] of cosmic rays has been associated with supernovae for a long time essentially due to their large energy output and because of the success of the phenomenon of diffusive shock acceleration [4], also known as the first-order Fermi acceleration mechanism, in accelerating particles up to energies $\sim 10^{15}$ eV (PeV). The energy reach of this process is further extended by invoking acceleration by shocks propagating through stellar and galactic winds. The expected nuclear composition of particles accelerated through different variants of this model is somewhat different and new measurements [5] may provide clues for resolving the mystery of the nature of the sources of ultra-high energy (UHE) cosmic rays.

Observational studies during recent years have focused on two aspects of UHE cosmic ray astrophysics, namely, direct studies on the sources of γ -rays and indirect studies on the nuclear composition of cosmic rays. Although the importance of studies [6–8] on cosmic γ -rays for very high energy (VHE) cosmic ray astrophysics was highlighted in the late 1940s and 50s, the field of VHE γ -ray astronomy [9] advanced only in 1980s following the breakthrough provided by the development of the imaging technique [10,11]. This was essentially due to an efficient rejection of the large background of charged cosmic rays. Similarly, at the UHE (10^{14} – 10^{16} eV), another breakthrough has been sought by the use of the muon component [12,13] for identifying γ -initiated showers in the presence of a large flux of showers

due to charged cosmic rays. The Chicago Air Shower Array (CASA) in association with the Michigan Muon Array (MIA) was the first experiment to use an array of large area muon detectors to search [14] for muon-poor showers as a signal from potential UHE γ -ray sources. The EAS-TOP [15], the KASCADE [16] and the GRAPES-2 [17] are the other recent experiments using either a large area muon detector or an array of muon detectors with the capability to observe muon-poor showers. However, the GRAPES-3 experiment [18,19,21] with its single large area (560 m^2) muon detector is attempting to reach a significantly higher level of sensitivity to γ -initiated showers based on their small muon content, particularly at sub-PeV energies, lower than those achieved by the CASA–MIA experiment. On the other hand, by using Čerenkov radiation in water as the particle detection mechanism, the MILA-GRO [22] experiment is attempting to achieve full particle detection sensitivity over a large area by instrumenting a 8 m deep water pond of $80 \times 60\text{ m}^2$ area with two layers of photomultipliers. The lower layer, located deeper in water, is used to detect the muons. However, reconstruction of particle (electron or muon) tracks in the MILA-GRO experiment is easier for smaller showers in the TeV (10^{12} eV) energy range and may be more complicated for showers in the PeV range.

Direct measurements [5] on the energy spectra of individual nuclei present in primary cosmic ray flux have been possible with satellite and balloon-borne detectors only up to a total energy $\lesssim 1$ TeV due to a steep fall in the flux with increasing energy and loss of accuracy in particle identification and energy measurement. The energy range has been extended to a total energy ~ 100 TeV by the use of nuclear emulsion and/or X-ray film as the detector element in shallow stacks of absorber flown aboard balloon platforms in long-duration flights [23,24]. These experiments have provided valuable data on the flux of groups of nuclei, for example, the CNO group, the Medium Heavy ($12 < Z < 20$) group and the Heavy ($Z \geq 20$) group. Due to severe practical constraints on the long duration flights with heavy payloads, studies in cosmic ray astrophysics at energies $\gtrsim 100$ TeV have to necessarily rely on indirect measurement of air showers

carried out at mountain altitude, sea level or underground locations. Due to combined effects of energy dependence of: (i) secondary multiplicity in particle interactions, (ii) interaction cross-sections of particles with air nuclei, (iii) decay life-time for kaons, pions, muons and (iv) nearly exponential nature of the density profile of the atmosphere, the muon component offers the highest sensitivity [17] for studies on the nuclear composition of primary cosmic ray flux at PeV energies. However the electrons, in an air shower being numerically dominant component, are used for obtaining information on various shower parameters, such as the arrival direction, the energy of the primary particle and also for generating a trigger.

The muon component has been studied in recent experiments in two different ways. Using an array of muon detectors, the muon size is determined for individual showers from an integration over the lateral distribution function as fitted to the observed muon densities, for example in the CASA-MIA [25] and KASCADE [16] experiments. Using a single large area muon detector, such as in the EAS-TOP experiment [15], the muon size has been estimated for individual showers from the lateral distribution function obtained from a fit to the data. On the other hand, the GRAPES-2 [17] group has made a detailed study of the muon multiplicity distribution in an attempt to obtain the flux of light nuclei (H+He+CNO groups) and heavy nuclei (Si+Fe groups) in cosmic rays almost independently. Pursuing the strategy of the GRAPES-2 group, the GRAPES-3 collaboration has constructed a large, 560 m² area, muon detector to study the muon multiplicity distribution for showers over a wide energy range.

The GRAPES-3 experiment is located at Ooty (11.4°N latitude, 76.7°E longitude and 2200 m altitude), a popular mountain resort town in southern India. The general layout of the GRAPES-3 muon detector is presented in Section 2 including the details of main detector element, namely the proportional counter (Section 2.1), the signal processing electronics and the data acquisition system (Section 2.2), and monitoring of the PRCs (Section 2.3). In Section 3 some of the observations showing the performance of the detector and its sensitivity for various kinds of

measurements are presented. In Section 4 the results from Monte Carlo simulations which demonstrate its potential for measurements on the nuclear composition of primary cosmic rays over PeV energy range are discussed. Finally, a summary is presented in Section 5.

2. The GRAPES-3 muon detector

Proportional counter (PRC) is the basic element of the GRAPES-3 muon detector. The PRC is a 600 cm long, mild-steel, square pipe with a cross-sectional area of 10 cm × 10 cm and a wall thickness of 2.3 mm as shown in Fig. 1.

A muon detector module with a sensitive area of 35 m² consists of a total of 232 PRCs arranged in 4 layers, with alternate layers placed in orthogonal directions. Two successive layers of PRCs are separated by 15 cm thick concrete, consisting of 60 cm × 60 cm × 15 cm blocks which permits a two-dimensional reconstruction of muon tracks in two vertical, orthogonal planes. The vertical separation of two layers of PRCs in the same plane is 50 cm which allows the muon track direction to be measured to an accuracy of ~6° in the projected plane.

To achieve an energy threshold of 1 GeV for vertical muons, a total thickness ~550 g cm⁻² in

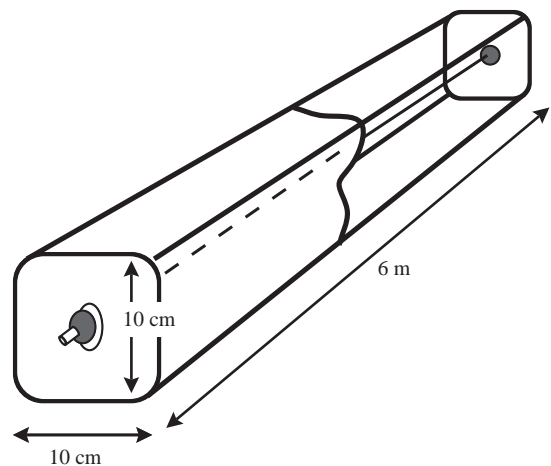


Fig. 1. A schematic diagram of 600 cm long PRC used as the basic detector element in the GRAPES-3 tracking muon detector.

the form of concrete blocks is employed as an absorber by placing a total of 15 layers of concrete blocks above Layer-1. The robust structure of the PRC permitted it, to support a huge load of 2.4 m thick concrete absorber in a self-supporting manner. The concrete blocks have been arranged in the shape of an inverted pyramid to achieve an energy threshold $1 (\sec \theta) \text{ GeV}$ for muons incident on the detector with zenith angle θ (with coverage up to 45°). A cross-section of two adjacent muon detector modules is shown schematically in Fig. 2. Four such modules, separated by a horizontal distance of 130 cm at the base, constitute one super-module.

Note that the top 7 layers of the concrete blocks are shared as an absorber by all four modules in a super-module. Therefore, the absorber above the 10th layer from the base, is essentially a full-size layer covering all four modules as seen in Fig. 2. Finally, a 30 cm thick and $18 \text{ m} \times 18 \text{ m}$ concrete slab was cast as the top layer of the absorber in order to make it weather-proof. Similarly at the bottom, a single 30 cm thick, $16 \text{ m} \times 16 \text{ m}$ concrete block cast on the ground, serves as the floor for the super-module. This has been done for uniform distribution of nearly 1200 t load of the absorber in a super-module to the soil below.

A picture of the PRCs and the concrete blocks in a super-module is shown in Fig. 3. The PRC-absorber assembly of each super-module has been enclosed within a large hall, with suitable doors and windows for access and illumination, and to control the humidity for safe operation of the PRCs. Two heavy duty de-humidifiers are operated round the clock, inside each of the four halls to maintain a low level of humidity ($< 50\%$), in

view of nearly eight month long rainy season at Ooty. Fig. 4 shows a picture of the four halls housing the super-modules of the muon detector. Some of the detectors of the GRAPES-3 shower array [21] which have been placed on the roof and around these halls are also visible.

2.1. Characteristic of PRCs

As described above, a muon detector is made up of 600 cm long PRCs. The pipe used for making a PRC, is closed at both ends with 6 mm thick, flat mild-steel plates equipped with hermetic, metal-to-glass seals and a gas valve. After welding of the end plates, the finished cross-section of the PRC had increased from $10 \text{ cm} \times 10 \text{ cm}$ to $10.2 \text{ cm} \times$



Fig. 3. An inside view of a super-module showing the proportional counters and layers of concrete blocks for two of the four modules. The remaining two modules are located further inside.

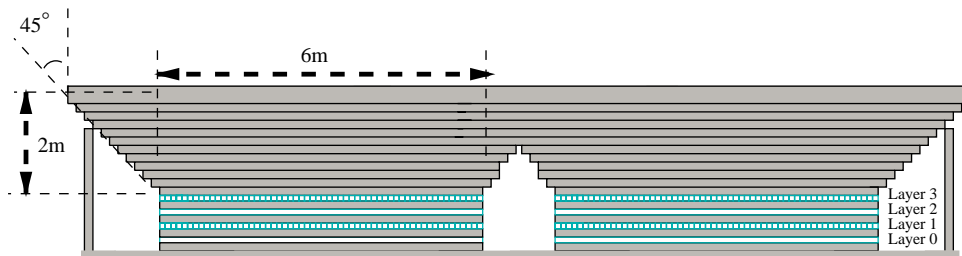


Fig. 2. Schematic of a muon detector module showing 4 layers of proportional counters embedded within concrete blocks.

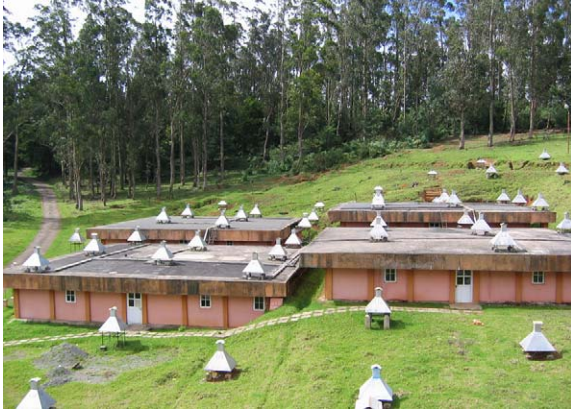


Fig. 4. A view of a part of the GRAPES-3 array showing the four halls housing the super-modules of the muon detector.

10.2 cm and therefore the 58 PRCs in a layer cover a distance of 5.92 m. After the deployment it has been found that the individual PRCs were aligned to within 2 mm and with a cumulative offset of $\lesssim 2$ mm from their designated nominal positions. The pipe also serves as the cathode of the PRC. A 100 μm diameter tungsten wire which also serves as the anode, is mounted at the center of the pipe using the hermetic seals.

After evacuation, each PRC is filled with P-10 (90% Ar and 10% CH_4) gas above local atmospheric pressure and then sealed. A schematic view of the PRC with its basic electronics, including a charge-sensitive pre-amplifier and a discriminator are shown in Fig. 5.

The amplitude distribution of the output pulses from each PRC has been measured with a multi channel analyzer. A typical distribution, shown in Fig. 6, displays a prominent peak due to cosmic ray muons corresponding to an energy loss of ~ 20 keV in the 10 cm column of P-10 gas in the PRC. The muon peak is well separated from the other two smaller peaks; the first peak is due to fluorescent K_α X-ray emission in Fe at 6.4 keV and the second minor peak at 8.6 keV is due to the same effect in the Zn coating on the mild steel pipe, used for its protection from rusting. Any malfunction of the PRC is easily detectable from a change in the shape of this distribution and suitable corrective steps can be initiated to restore its performance.

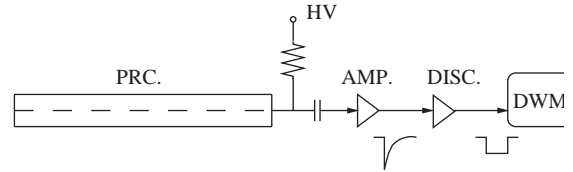


Fig. 5. A schematic diagram of PRC and associated electronics used as the basic detector element of the tracking muon detector.

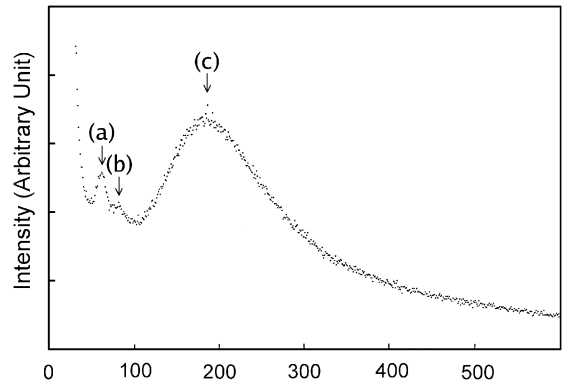


Fig. 6. Pulse-amplitude distribution for a PRC in the muon detector. The first two minor peaks are due to fluorescent K_α X-ray emission in Fe at 6.4 keV (a), and in Zn at 8.6 keV (b). The main peak at ~ 20 keV (c) is due to the passage of cosmic ray muons.

The anode pulse from the PRC is shaped to an exponential form with a decay time of $7 \mu\text{s}$ and amplified (gain = 83). The amplified pulse is discriminated at a threshold of -100 mV which corresponds to ~ 0.2 of a minimum ionizing particle. The output of the discriminator is a TTL signal. The following information on the discriminator output pulse is recorded; (i) the arrival time with a resolution of 167 ns and (ii) the width with a resolution of 333 ns. Due to exponential nature of the amplified pulse, the pulse width is proportional to the logarithm of the PRC pulse amplitude.

The number of particles passing through a PRC in a given event are estimated as follows, assuming T_s to be the pulse-width for a minimum ionizing particle, as calculated from the pulse-width monitoring system and τ to be the decay time constant, the number of particles N in an event is given by

$$N = e^{(T_n - T_a)/\tau} \quad (1)$$

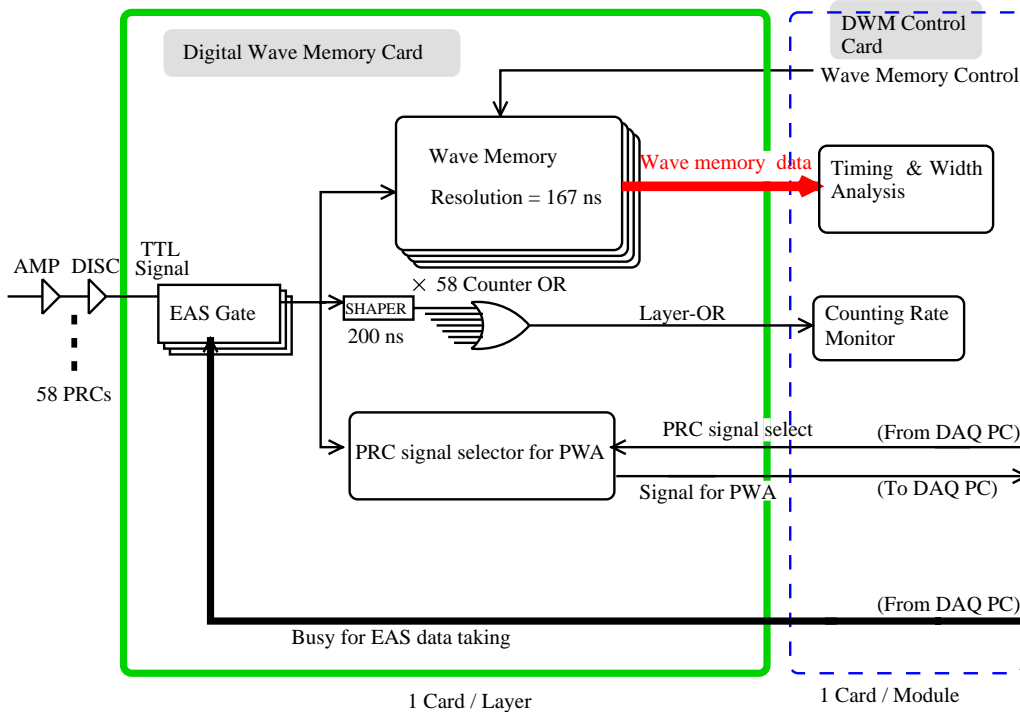


Fig. 8. Block diagram of the DWM card. Each card handles TTL signals from one layer of 58 PRCs. Also shown is the DWM control card.

the DWM card freezes the contents of all RAM chips, after a preset delay of $79\ \mu\text{s}$. Since at any instant the DWM card holds information on PRC pulses for the previous $85\ \mu\text{s}$, the preset delay of $79\ \mu\text{s}$ allows data corresponding to $85 - 79 = 6\ \mu\text{s}$ prior to the arrival of the shower trigger to be accessed. Due to exponential shaping of PRC output pulse, the number of successive 167 ns intervals with logic state '1' provides direct measure of the logarithm of pulse height. The PRC signals are sampled for $6\ \mu\text{s}$ before the arrival of muons, since it takes $2\ \mu\text{s}$ to generate the trigger after the passage of a shower. The shower trigger switches the DWM card to READ mode and starts the transfer of data to the DWM control card.

For further processing, each PRC pulse is re-shaped into a TTL pulse of width 200 ns and an OR of all re-shaped pulses in a layer, termed 'Layer-OR', is generated. The performance of PRCs in a layer is monitored by taking various

combinations of coincidences among the layers. These coincidences between the Layer-OR signals have an excellent sensitivity to the performance of PRCs in a module.

2.2.2. DWM control card

Fig. 9 shows the block diagram of the DWM control card. This card has been designed to take care of the signals from the four DWM cards of a module. The control card serves the following functions after receiving a shower trigger:

- (1) Reads the stored signals, including the arrival time and pulse-width information from DWM cards for each layer.
- (2) Monitors the rate of each Layer-OR and all combinations of coincidences among Layer-OR signals.

Observations have shown that most of the muons unassociated with the recorded shower can be

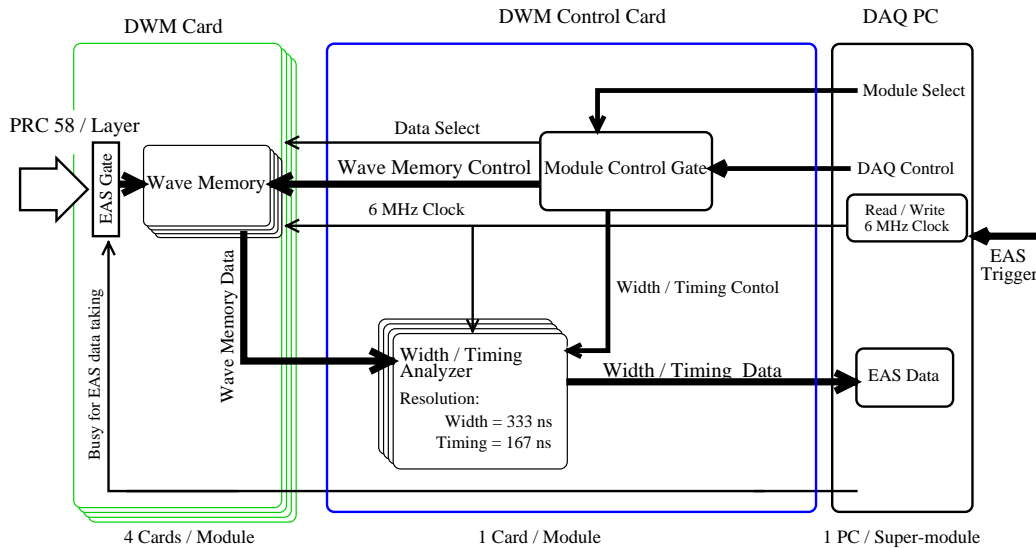


Fig. 9. Block diagram of the DWM control card which starts recording of PRC data, following the receipt of a trigger from the shower array. Also shown are DWM card and DAQ-PC used for data recording.

identified and rejected, just with a strict cut on the recorded arrival time of muons, without taking into account the arrival direction of the shower. This reduces the probability of observing accidental muons (for a 3-layer hit) to $\lesssim 0.2$ muons per shower.

2.2.3. Data acquisition PC

A pair of I/O interface cards inserted in the DAQ-PC handle all four DWM control cards in a super-module. On the receipt of the shower trigger from the GRAPES-3 array, the DAQ-PC sends a command to freeze the contents of DWM cards and subsequently transfers these data to the DWM control card. The data in the DWM control card is then written on a hard disk along with the time stamp having an accuracy of $1 \mu\text{s}$. The time stamp is generated from a real-time clock, running on a good quality, 10 MHz quartz oscillator. The real-time clock is synchronized using a GPS receiver every second. The muon data and the air shower data, which are recorded independently, are collated during analysis by using the time stamps recorded at the four muon super-modules and the shower array. A sample of the observed muon tracks in a typical air shower is shown in Fig. 10.

The dead-time due to the data acquisition process is about 5 ms per shower. Since the shower trigger rate is ~ 13 Hz, it contributes to a dead time fraction of $\sim 7\%$. On an average around 400 bytes are required for recording a shower for the triggering conditions mentioned later. These data are temporarily stored into a local hard disk in the DAQ-PC for various checks and are subsequently recorded on a CD or DVD for permanent storage and off-site analysis.

2.3. Monitoring of the performance of PRCs

The maintenance of the stability of gain and detection efficiency of each PRC is an important experimental requirement. In order to monitor the performance of the muon detector, the pulse-width of all 3712 PRCs is continuously measured with a pulse width analyzer system. A typical pulse-width distribution is shown in Fig. 11. Note that as a result of exponential shaping of PRC pulse and subsequent measurement of its width, the number of 'equivalent' minimum ionizing particles entering a PRC are effectively digitized to an accuracy of $\sim 5\%$ for 1–5 particles and $\sim 10\%$ for more than 5 particles. The shape of the pulse-width distribution is utilized to detect noisy and/or leaky PRCs.

Run No. 018543 Event No. 006157 20010410 14:32:41.86946

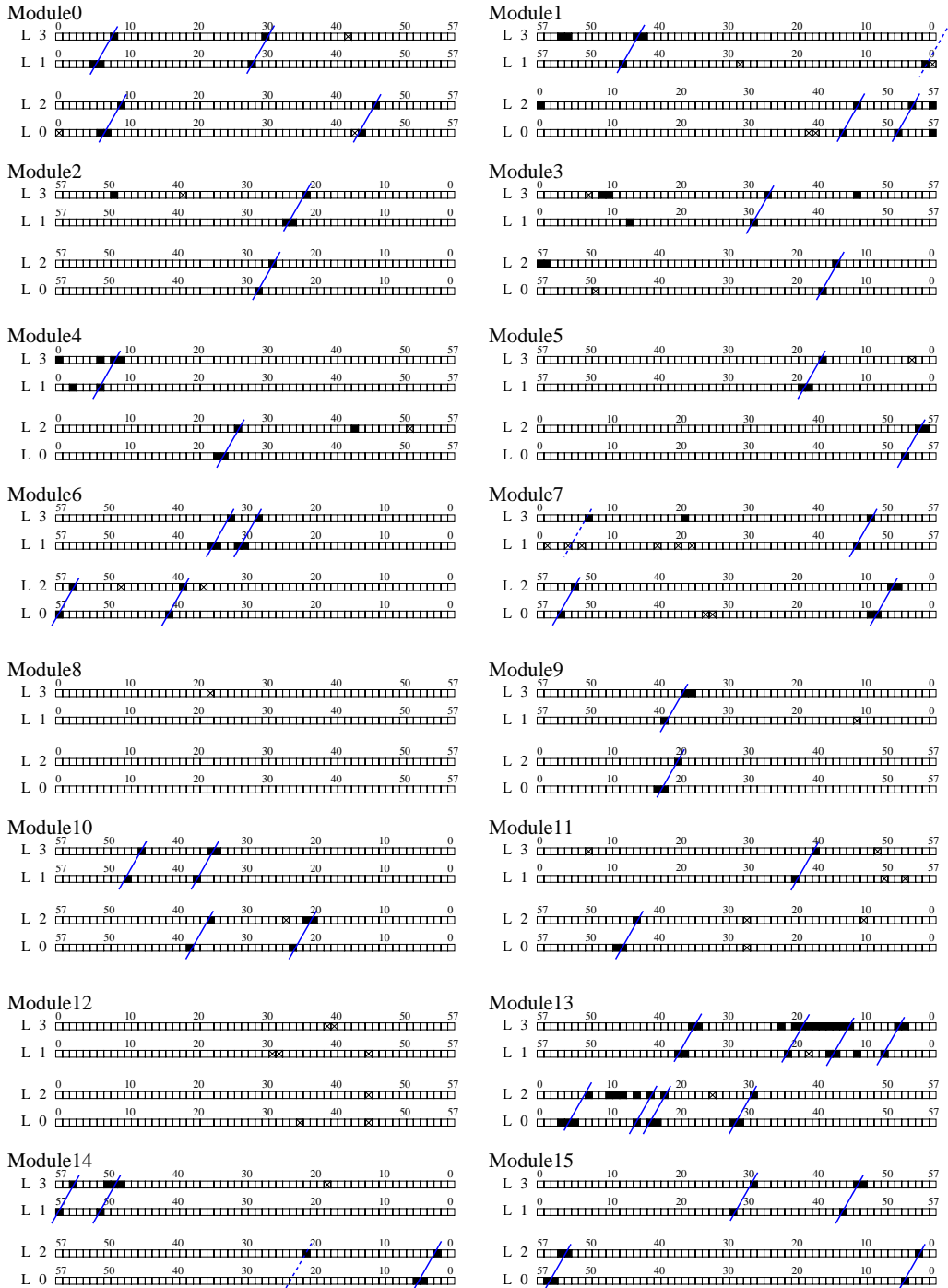


Fig. 10. Muon tracks associated with a typical air shower. The PRCs hit are represented by ■ and straight lines joining these ■ represent the muon tracks. A pair of lines, (L0–L2) and (L1–L3), represent two orthogonal views of each muon track. A total of 24 muons tracks could be reconstructed for this shower.

The 6.4 keV fluorescent K_{α} X-ray emission peak in Fe is used for calibration and monitoring of the gain of the PRCs. In addition, the counting rates of any 3-layer and all 4-layer coincidences between Layer-OR signals are also monitored continuously

to provide information on the health of the muon detector.

In Fig. 12, a schematic diagram of the monitoring of the Layer-OR rate in DWM control card is shown. The multi-layer rate is very sensitive to some of the atmospheric parameters, such as the barometric pressure and the temperature profile in the upper atmosphere. The detected muon rate is also affected by the influence of the inter-planetary magnetic field and the solar wind on the propagation of relatively lower energy ($\lesssim 10^{11}$ eV) primary cosmic rays.

In Fig. 13, the variation in muon flux through N -layer coincidence rate ($N = 3$ or 4), atmospheric pressure and temperature for a period of seven days during 7–14 March 2001 are shown. The temperature data shows a periodicity of one cycle per day due to the solar heating. However, the pressure and muon rate data show a periodic variation of 2 cycles per day. In Fig. 13, the 12 h periodicity is seen in the muon rate from any 3-layers (a) in the top panel with an amplitude of $\sim 0.3\%$, for all 4-layers, (b) in the second panel

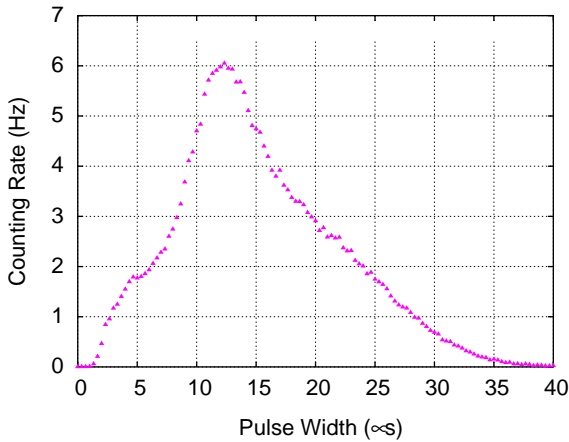


Fig. 11. A typical pulse width distribution for a PRC in the muon detector.

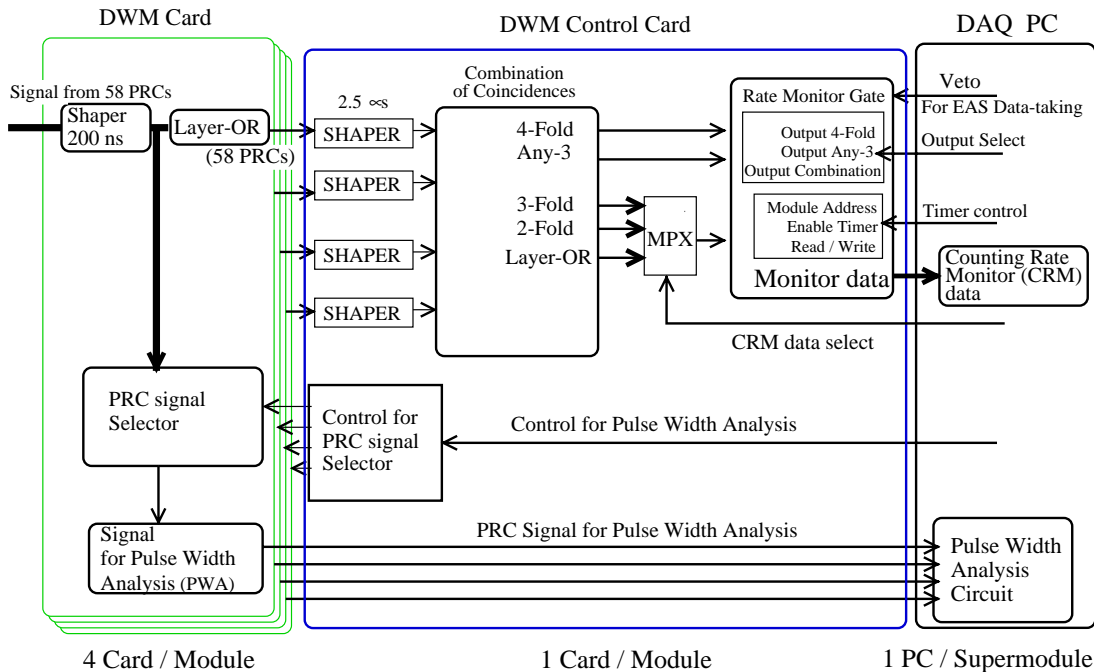


Fig. 12. Block diagram of monitoring system in the DWM control card. Also shown are DWM card and the DAQ-PC.

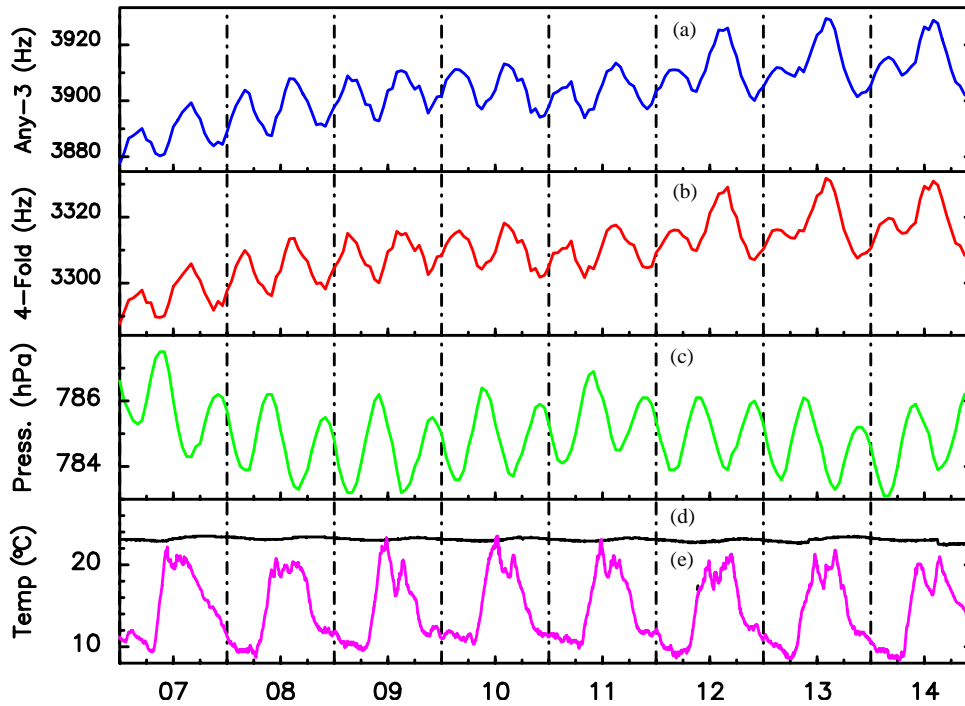


Fig. 13. Observed variations over a seven day period during 7–14 March, 2001; (a) any 3-layer coincidence rate in Hz, (b) 4-layer coincidence rate in Hz, (c) atmospheric pressure in hPa, (d) temperature inside a muon hall and (e) temperature outside muon halls.

with same amplitude ($\sim 0.3\%$) and in atmospheric pressure, (c) in the third panel with an amplitude of $\sim 0.2\%$. The last panel in Fig. 13 shows that the temperature inside a muon hall, (d) remains almost constant to within 0.2°C , however the temperature outside muon halls, and (e) shows significant variation ($8\text{--}22^\circ\text{C}$) dependent on the local weather.

The periodic variation of two cycles per day in the pressure data is a well-known phenomenon at low latitudes. An anti-correlation between the pressure wave and the muon counting rates is clearly visible in Fig. 13. This anti-correlation can be explained in terms of a change in the atmospheric absorption of muons due to the pressure wave. These observations are of critical importance while analyzing data, for studying various transient phenomena, including those due to cosmic, solar [20] or atmospheric origin. The pressure effect is also clearly seen in the shower counting rate [21].

Due to its large area, the GRAPES-3 muon detector rate, after correction for the changes in the atmospheric pressure, has been observed to be nearly constant with an rms variation of $\sim 0.1\%$. This enables the GRAPES-3 muon detector to be a very sensitive monitor of the Solar activity, particularly, for observations on phenomena such as Ground Level Enhancements (GLEs) and Forbush decreases. Fig. 14 shows a remarkable decrease of almost 10% in the cosmic ray muon flux, on the morning of 29 October, 2003, ~ 20 h after a large X17 class solar flare on 28 October, 2003. In fact the muon flux had started to decrease from 22 October, 2003, almost six days prior to the onset of the large Solar flare at 09:51 Hrs UTC on 28 October, 2003, indicated by the first (\blacktriangledown) marker in Fig. 14, and before the arrival of the coronal mass ejection (CME) at the Earth at 06:13 Hrs UTC, on 29 October, 2003 as indicated by the second (\blacktriangledown) marker in the same figure. The muon flux continued to display large variation over this

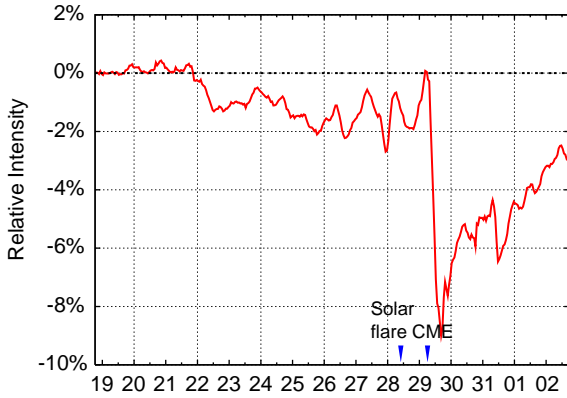


Fig. 14. Variation in the muon (4-layer) rate over a two week period in October–November 2003 overlapping occurrence of a X17 class Solar flare at 9:51 Hrs UTC on 28 October indicated by first marker and arrival of CME at the Earth at 6:13 Hrs UTC on 29 October indicated by second marker.

six day period along with a systematic decrease $\sim 2\%$ of the quiescent flux. The observed muon flux continued its exponential recovery beyond 2 November, 2003, reaching its pre-Forbush decrease level by 10 November, 2003. In fact, a lot more instrumentation has been added to the GRAPES-3 muon detector to enable detailed studies on cosmic ray flux variations related to the solar phenomenon whose details are discussed elsewhere [20,26,27].

3. Observations and expectations

Due to sensitivity of the PRCs to low energy γ -rays from radioactivity in the concrete absorber, the counting rate of individual PRCs is quite large, ~ 200 Hz. Also, the PRC is a relatively slow detector with a pulse rise time ~ 500 ns. The decay time of the pulse has been adjusted to be $7 \mu\text{s}$ to enable an accurate measurement of pulse amplitude through digitization of the pulse-width. Due to these two factors, there is a small but non-negligible probability that a few PRCs are fired randomly with each shower trigger. However, the accidental muon rate is reduced to $\lesssim 0.2$ per shower by a cut of $\pm 3 \mu\text{s}$ relative to the shower trigger, on the time of arrival of muons.

In addition, a comparison of the direction of a muon track with that of shower helps in further reducing the number of accidental muons. The angular resolution of the muon detector is $\sim 6^\circ$ in each of the two projected planes. It has been observed that by putting the requirement that the direction of the re-constructed muon track should match the projection of the arrival direction of the shower to within 10° , the number of PRCs triggered by muons, unrelated to the shower is reduced to $\lesssim 0.07$ per shower [28].

The estimate of the number of muon tracks in each module is quite accurate for a small number of muons. The layer efficiency has been independently estimated and is found to be $> 98\%$. After allowing for the small gaps between the PRCs, the missing probability is estimated to be $< 0.3\%$ for single muon tracks in a module. Based on the layer efficiency of $> 98\%$, the muon detection efficiency is estimated to be $> 92\%$ for all 4-layer and $> 99.8\%$ for any 3-layer coincidences, respectively. However, the number of muons is generally underestimated if the number incident on a module is large. This is due to the fact that two muons incident on the adjacent PRCs are likely to be counted as one, particularly at larger zenith angles. Using a simple track-finding algorithm and random distribution of muons, simulations have shown that the under-estimate becomes as large as 20% when the number of muons exceeds 10 in a single module. However, this factor is taken into consideration during data analysis through a response function obtained from simulations.

4. Simulations of muon multiplicity distribution

It is well-known that the protons constitute the largest fraction of primary particles for showers which are selected using a trigger based on density of particles which are predominantly electrons near the core. While the electron component of a shower, as observed in the lower atmosphere, is relatively insensitive to the atomic number of the primary cosmic ray particle, the muon multiplicity is one of the most sensitive parameters for determining the atomic number of the primary particle initiating the shower. Therefore it is

important to study muon multiplicity distributions for various triggering conditions used for selecting showers.

Fig. 15 shows the muon multiplicity distribution for showers selected with 3-line coincidence trigger which also requires the triggering of an additional 7 detectors from those located within the inner 127 detectors of the array [21]. In a large sample of showers, the total number of detected particles is proportional to the total number of particles in the shower at the observational level (shower size), which in turn is proportional to the energy of the primary particle. Thus the total number of detected particles represents, the primary energy on a statistical basis. Thus a further cut on the total number of detected particles Σn_i , of $50 \leq \Sigma n_i \leq 100$ is also imposed. The expected muon multiplicity distributions were generated from Monte Carlo simulations using the CORSIKA code [29] and QGSJet model [30] for hadronic interactions. For a comparison, the muon multiplicity distributions for γ -ray, proton and Fe initiated showers are also shown in Fig. 15. The energy of γ -ray, proton and Fe primary were generated by assuming that the flux in each case is represented by the same differential power law spectrum ($E^{-2.7}$). For each of the distributions in

Fig. 15, the total number of showers has been normalized to be 1.

It is interesting to note that the experimentally observed distribution (a) in Fig. 15 lies between the expected distributions for proton (c) and iron (d) primaries. Clearly, the observed distribution shown in Fig. 15 requires a significant contribution of heavier nuclei. This discrimination based on the atomic number is made possible because the showers initiated by heavier nuclei such as iron generate a much larger number of muons as compared to lighter nuclei such as proton and He. It has also been shown through simulations [17] that larger muon multiplicities are predominantly due to the contribution of medium heavy and heavy nuclei in the primary flux, when showers are selected through a well-defined criterion for the shower particles, such as particle-sum, etc. It is this sensitivity of different multiplicity regions to different nuclear groups which is expected to enable a determination of the relative contribution of each nuclear group to the primary cosmic ray flux.

A use of the muon-poor criterion for showers is expected to reject hadron induced showers efficiently when data from a large muon detector is used. From the γ -ray simulations shown in Fig. 15, it is estimated that $\geq 90\%$ of hadron induced showers can be rejected with a selection of showers where no muon is detected, while only a few percent of γ -ray induced showers get rejected with this cut. This provides a powerful tool while searching for cosmic sources of UHE γ -rays.

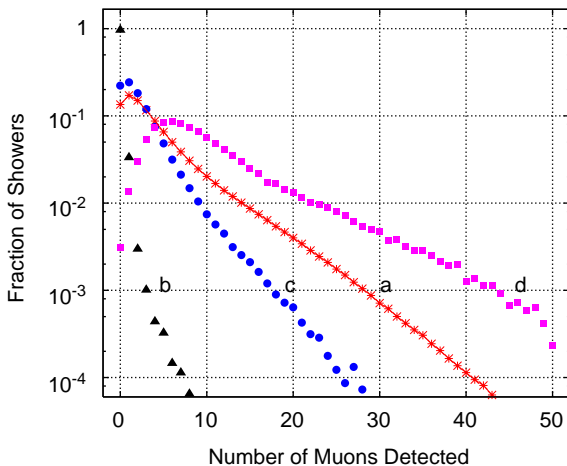


Fig. 15. (a) The observed muon multiplicity distribution for showers is shown using * with a cut on the ‘particle-sum’ Σn_i , $50 \leq \Sigma n_i \leq 100$. Monte Carlo simulations with the same cut are shown, (b) γ -ray primaries using \blacktriangle , (c) proton primaries using \bullet and (d) Fe primaries using \blacksquare .

5. Summary

In this paper, detailed features of the GRAPES-3 muon detector have been presented. The area of 560 m^2 makes it one of the largest tracking muon detectors in the world. The unique features of the detector electronics makes it possible to measure the pulse arrival time and width for each PRC where a muon has traversed. The arrival time of each muon, measured to an accuracy of 167 ns, makes it possible to reject most of the muons which are physically unassociated with a shower. The angular resolution of the muon detector is

$\sim 6^\circ$ in each of the two projections. A comparison of the muon direction with that of the shower in two orthogonal projections, further reduces the background of unassociated muons to a negligible level.

In cases where more than one muon has passed through a PRC, the pulse-width is used to estimate the total number of muons. Using an efficient track reconstruction algorithm, the total number of ≥ 1 GeV muons incident on the detector can be estimated to a reasonable accuracy up to a maximum of 160 muons. Using muon multiplicity distributions, it is expected that the mass composition of cosmic rays can be measured accurately in the energy range from 3×10^{13} – 3×10^{16} eV. A cut on the muon content in a shower permits an efficient rejection ($\geq 90\%$) of hadron induced showers and a preferential selection of γ -ray induced showers, during the search for cosmic γ -ray sources above 10^{13} eV.

Acknowledgements

We thank D.B. Arjunan, K. Manjunath, B. Rajesh and C. Ravindran for their help in testing, installation and operation of the proportional counters and the electronic modules. The administrative services of V. Viswanathan during all phases of the experiment are gratefully acknowledged. It is a pleasure to thank A.A. Basha, G.P. Francis, I.M. Haroon, V. Jeyakumar, A. Pushpanathan and K. Ramadass for their help in the fabrication, assembly and installation of various mechanical components and detectors. We also thank M.A. Ali, P. Amalraj, M. Iyer, B. Jasper, G.C. Kamat, A. Pratheep, T.T. Sreedevi and S. Thirunavukkarasu for their help during certain phases of the experiment. The Japanese members of the GRAPES-3 collaboration acknowledge the partial financial support from the Ministry of Education and Science of the Government of Japan for the experiment. The GRAPES-3 collaboration thanks N.K. Mondal, V.S. Narasimham and their colleagues in the TIFR-OCU Proton Decay Collaboration for the loan of the proportional counters which have been used in the muon detector.

References

- [1] V.S. Berezhinskii, et al., *Astrophysics of Cosmic Rays*, North-Holland, Amsterdam, 1990.
- [2] P.L. Biermann, T.K. Gaisser, T. Stanev, *Phys. Rev. D* 51 (1995) 3450;
B. Wiebel-Sooth, et al., *Astron. Astrophys.* 330 (1998) 389;
P.L. Biermann, G.M. Tanco, *Nucl. Phys. B* 122 (Proc. Suppl.) (2003) 86.
- [3] A.D. Erlykin, A.W. Wolfendale, *J. Phys. G: Nucl. Part. Phys.* 27 (2001) 941;
A.D. Erlykin, A.W. Wolfendale, *J. Phys. G: Nucl. Part. Phys.* 27 (2001) 959;
A.D. Erlykin, A.W. Wolfendale, *J. Phys. G: Nucl. Part. Phys.* 27 (2001) 1709.
- [4] L. O'C Drury, *Rep. Prog. Phys.* 46 (1983) 973;
M.A. Malkov, L. O'C Drury, *Rep. Prog. Phys.* 64 (2001) 429.
- [5] J.P. Wefel, et al., *J. Phys. G: Nucl. Part. Phys.* 29 (2003) 821.
- [6] E. Feenberg, H. Primakoff, *Phys. Rev.* 73 (1948) 449.
- [7] S. Hayakawa, *Prog. Theoret. Phys.* 8 (1952) 571.
- [8] P. Morrison, *Nuovo Cimento* 7 (1958) 858.
- [9] R.A. Ong, *Phys. Rep.* 305 (1998) 93.
- [10] A.M. Hillas, *Proceedings of the 19th ICRC*, vol. 3, La Jolla, 1985, p. 445.
- [11] M.F. Cawley, *Exp. Astron.* 1 (1990) 173;
M.F. Cawley, T.C. Weekes, *Exp. Astron.* 6 (1995) 7;
D.J. Fegan, *J. Phys. G: Nucl. Part. Phys.* 23 (1997) 1013.
- [12] T.K. Gaisser, et al., *Phys. Rev. D* 43 (1991) 314.
- [13] S. Mikocki, et al., *J. Phys. G: Nucl. Part. Phys.* 17 (1991) 1303.
- [14] J.W. Cronin, et al., *Phys. Rev. D* 45 (1992) 4385;
T.A. McKay, et al., *Astrophys. J.* 417 (1993) 742;
A. Borione, et al., *Astrophys. J.* 481 (1997) 313;
A. Borione, et al., *Phys. Rev. D* 55 (1997) 1714.
- [15] M. Aglietta, et al., *Astropart. Phys.* 3 (1995) 1;
M. Aglietta, et al., *Astropart. Phys.* 6 (1996) 71;
M. Aglietta, et al., *Astropart. Phys.* 10 (1999) 1.
- [16] T. Antoni, et al., *Astropart. Phys.* 14 (2001) 245.
- [17] S.K. Gupta, et al., *Phys. Rev. D* 68 (2003) 052005.
- [18] N. Ito, et al., *Proceedings of the 25th ICRC*, vol. 7, Durban, 1997, p. 225
Y. Hayashi, et al., *Proceedings of the 26th ICRC*, vol. 1, Salt Lake City, 1999, p. 236.
- [19] Y. Hayashi, et al., *Proceedings of the 26th ICRC*, vol. 1, Salt Lake City, 1999, p. 276
Y. Hayashi, et al., *Proceedings of the 27th ICRC*, vol. 1, Hamburg, 2001, p. 111.
- [20] S. Kawakami, et al., *Proceedings of the 26th ICRC*, vol. 7, Salt Lake City, 1999, p. 171
S. Kawakami, et al., *Proceedings of the 27th ICRC*, vol. 9, Hamburg, 2001, p. 3473
H. Kojima, et al., *Proceedings of the 27th ICRC*, vol. 10, Hamburg, 2001, p. 3943
T. Nonaka, et al., *GRAPES-3 Preprint 2004c*, to be published.

- [21] S.K. Gupta, et al., *Nucl. Instr. and Meth. A* 540 (2005) 311.
- [22] R. Atkins, et al., *Nucl. Instr. and Meth. A* 449 (2000) 478; R. Atkins, et al., *Astrophys. J.* 595 (2003) 803.
- [23] K. Asakimori, et al., *Astrophys. J.* 502 (1998) 278.
- [24] A.V. Apanasenko, et al., *Astropart. Phys.* 16 (2001) 13.
- [25] A. Borione, et al., *Nucl. Instr. and Meth. A* 346 (1994) 329; M.A.K. Glasmacher, et al., *Astropart. Phys.* 10 (1999) 291; M.A.K. Glasmacher, et al., *Astropart. Phys.* 12 (1999) 1.
- [26] T. Nonaka, et al., *Proceedings of the 28th ICRC*, vol. 6, Tsukuba, 2003, p. 3569.
- [27] H. Kojima, et al., *Proceedings of the 28th ICRC*, vol. 7, Tsukuba, 2003, p. 3913; H. Kojima, et al., *Proceedings of the 28th ICRC*, vol. 7, Tsukuba, 2003, p. 3957.
- [28] Y. Hayashi, et al., *Proceedings of the 28th ICRC*, vol. 4, Tsukuba, 2003, p. 2273.
- [29] D. Heck, et al., *CORSIKA, A Monte Carlo Code to Simulate Extensive Air Showers*, Forschungszentrum Karlsruhe FZKA, vol. 6019, 1998; D. Heck, et al., *Proceedings of the 27th ICRC*, Hamburg, 2001, p. 233.
- [30] N.N. Kalmykov, S.S. Ostapchenko, A.I. Pavlov, *Nucl. Phys. B* 52B (Proc. Suppl.) (1997) 17.